ANNALS OF GEOPHYSICS, 67, 3, SE319, 2024; doi: 10.4401/ag-9033
OPEN ACCESS

GINGER data analysis for seismology

Andrea Basti[1], Giorgio Carelli[1], Giuseppe Di Somma[1], Enrico Maccioni[1], Paolo Marsili[1], Nicolò Beverini[2], Simone Castellano[*,3], Gaetano De Luca[4], Angela Di Virgilio[5], Daniela Famiani[6], Aladino Govoni[6]

(1) Dipartimento di Fisica, Università di Pisa, Italy, and Istituto Nazionale di Fisica Nucleare (INFN), sezione di Pisa, Pisa, Italy
(2) Dipartimento di Fisica, Università di Pisa, Pisa, Italy
(3) Istituto Nazionale di Fisica Nucleare (INFN), sezione di Pisa, Italy, and Gran Sasso Science Institute, L'Aquila AQ, Italy
(4) Istituto Nazionale di Geofisica e Vulcanologia, Sez. ONT. sede di L'Aquila, L'Aquila AQ, Italy
(5) Istituto Nazionale di Fisica Nucleare (INFN), sezione di Pisa, Pisa, Italy
(6) Istituto Nazionale di Geofisica e Vulcanologia, sezione ONT, Roma, Italy

Article history: received October 30, 2023; accepted June 26, 2024

Abstract

Since several years, the ring laser gyroscope GINGERINO is operative inside the underground Gran Sasso laboratory. It monitors on a continuous basis the local Earth angular velocity in the horizontal plane. It provides unique information for geophysics in general, being one of the few top sensitivity angular velocity sensors. The present paper describes the analysis procedure developed for the data uploaded on the EIDA data base, suitable for seismological investigation in the frequency window 100 s up to 100 Hz. Typical errors and data quality will be discussed. This work is part of the data analysis tools under development for the GINGER project, a ring laser array, part of the UGSS (Underground Gran Sasso Seismology) multi components array at present in construction inside the Gran Sasso laboratory.

Keywords: Ring laser; 4C seismology; Sagnac effect; Frequency reconstruction; Geodesy

1. Overview of the instrument, and its application in seismology

Rotational seismology is an emerging field, involving all aspects of rotational motions induced by earthquakes, explosions, and ambient vibrations. It is of interest to several disciplines, including seismology, earthquake engineering, geodesy, and gravitational waves [Belfi et al., 2017; Yuan et al., 2020; Simonelli et al., 2016; Simonelli et al., 2018; Simonelli et al., 2020; Simonelli et al., 2021; rot.seism.; Igel et al., 2021; Zembaty et al., 2021; Bernauer et al., 2021]. The addition of rotational degrees of freedom to traditional seismometers makes up to 6-components (6C) single-point observations possible; a single 6C observation, for instance, allows to derive properties of the seismic wavefield for which classical 3C seismology needs arrays of multiple translational sensors [Zembaty et al., 2021]. Among a vast new-generation of rotational sensors [Bernauer et al., 2021], Large area Ring Laser Gyroscopes (RLGs) can measure the fast component of the frame angular velocity, with unprecedented sensitivity. A RLG schematic view is shown in Figure 1. Its working principle is based on the Sagnac effect. When

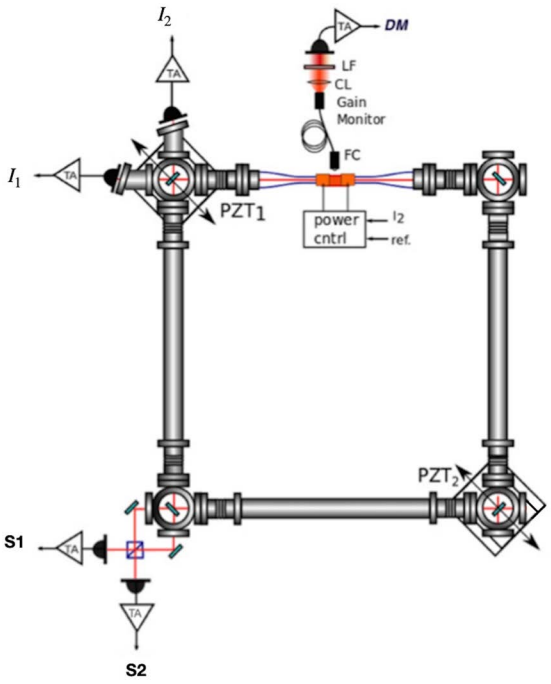

Figure 1. Schematic view of a Ring Laser Gyroscope (RLG). In particular, raw data acquired are the two laser mono-beams (PH1, PH2), and two beat note signals.

the optical cavity of a ring laser is rotating around its axis, the time of round trip of the light beam co-rotating with the cavity is slightly increased, while that of the counter-rotating one is slightly decreased. Then, a small frequency difference is produced between the two beams traveling in the opposite directions. This frequency difference, named Sagnac frequency (f_s), is proportional to the frame rotational velocity Ω, and can be observed as the beat note between the two beams on a photo-detector:

$$f_s = \frac{4A}{\lambda L} \cdot \Omega \cdot \cos(\theta) = S \cdot \Omega \cdot \cos(\theta), \tag{1}$$

where A is the area of the ring cavity, L is its perimeter, λ the wavelength of the light, and θ is the angle between the area versor of the ring and the orientation of Ω. For RLGs horizontally aligned (area versor vertical) θ is the colatitude angle, while for RLGs aligned at the maximum Sagnac signal $\theta = 0$. Equation 1 connects Ω with f_s by means of the scale factor $S = \frac{4A}{\lambda L}$, and θ. In the case of GINGERINO, lying horizontally in Gran Sasso laboratory, $L = 14.4$ m, and $\theta \simeq 47°33'$ is the colatitude angle. For a RLG rigidly fixed to the ground, the local vertical rotation Ω_z is dominated by the Earth angular velocity projected on the gyroscope axis, $\Omega_\oplus \cdot \cos(\theta)$. Ω_z keeps track of any local variations to such angular velocity, as can be slow or fast vibrations or noises of any nature, arising from close or far sources.

The measured beat note pulsation (ω_m from here on) as reconstructed by Hilbert algorithm is however affected by laser non linear dynamics and some corrections must be done, in order to obtain the true value of $\omega_s = 2\pi f_s$. As reported in [Di Virgilio et al., 2019], this can be made recording as additional diagnostic signals the intensity of the two laser beams (the so called mono-beam signals, Fig. 1). The procedure is described in the following paragraphs.

As an example of tele-seismic event detected by GINGERINO, the event from the 2023 Turkey sequence is shown in Figure 2; the rotational component is seen by GINGERINO, the East-West, North-South, and z components are seen by GIGS, the colocated seismic station. IV.GIGS is a Very Broad Band (VBB) seismic station managed by INGV, equipped with a Nanometrics Trillium 240 s and a Centaur data logger. GINGERINO data shown in this image have a bandwidth of 10 Hz for a better imaging. It can be noticed that in the GINGERINO plot there are 2 small spikes before the important tele-seismic event. The first spike has been identified as a small local earthquake, of seconds duration, the second spike as a local noise; they are not visible in the 3 GIGS plots, which show raw data from HHE, HHN, and HHZ channels, respectively; the signal in GIGS, in fact, has low frequency variations greater in amplitude

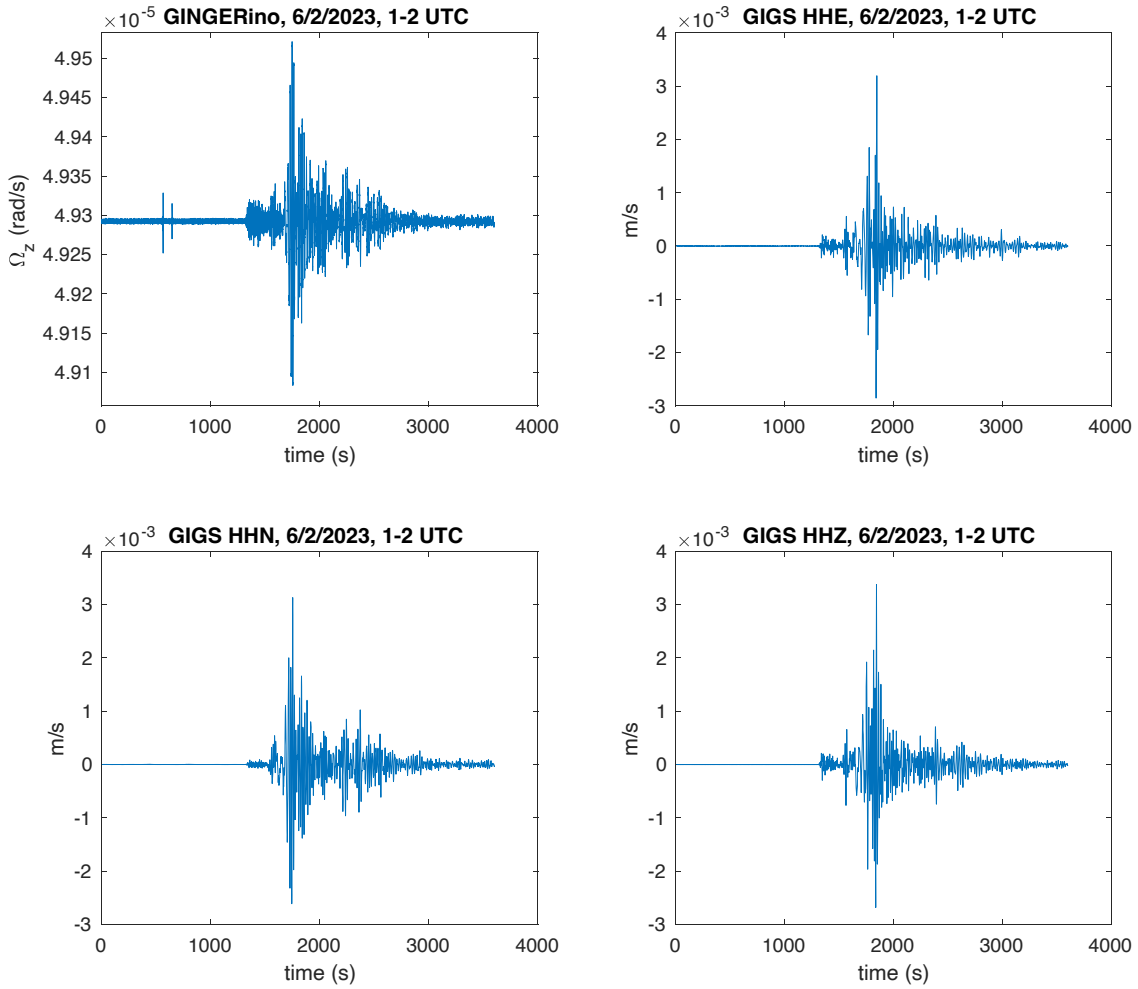

Figure 2. Seismic event seen by GINGERINO (top left), Turkey, February 6th, 2023, compared to the same event seen by the co-located seismic station GIGS, East-West component (top right), North-South component (bottom left), z component (bottom right). The mean value in the GINGERINO plot was not subtracted, in order to show the measured Earth angular velocity. Plots show one hour of data, from 1:00 to 2:00 UTC.

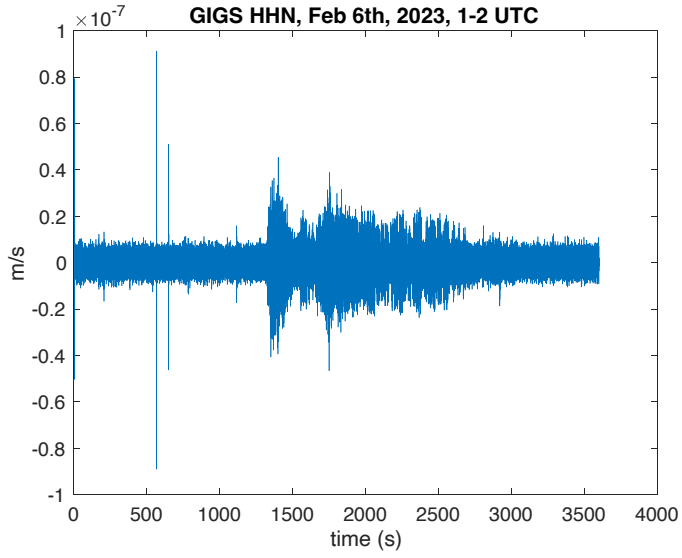

Figure 3. Seismic event seen by GIGS, North-South component; in this case, a band pass filter (5-15 Hz) was applied to GIGS data. Plot shows one hour of data, from 1:00 to 2:00 UTC.

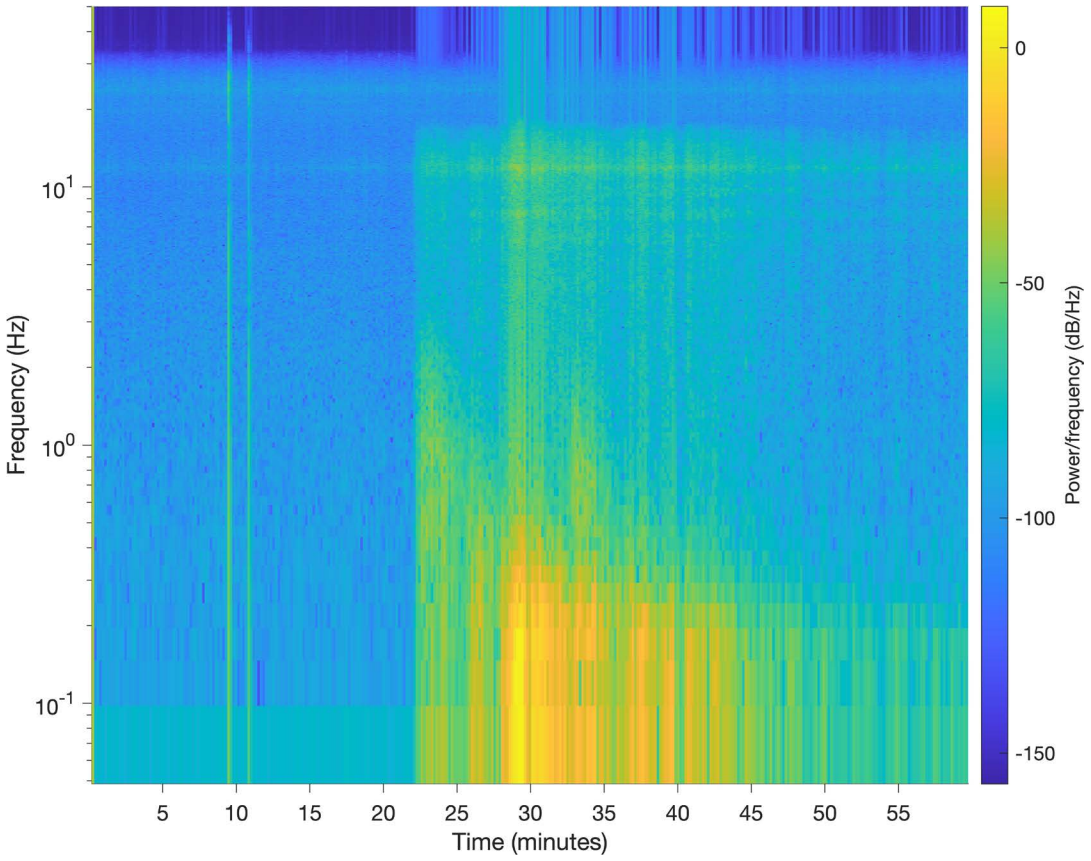

Figure 4. Spectrogram of the Turkey seismic event seen by GINGERINO, 6 Feb 2023. We are able to notice the different frequency range of the two local events and the teleseismic Turkey event. The effect of the band pass filter (280 ± 12) Hz utilized to process such portion of data is visible.

than such events, below 5 Hz, and a white noise up to high frequencies which is not much lower than such signals. By applying to GIGS data a suitable band-pass filter (5-15 Hz in this case), the large tele-seismic event is reduced in amplitude (in all its 3 components), while the two spikes are now visible (Fig. 3, the filtered HHN component); local vibrations have, in fact, higher frequency content with respect to tele-seismic events, where higher frequencies are filtered out during wave propagation. In Figure 4, a spectrogram of the tele-seismic event seen by GINGERINO is shown. The local vibrations are also visible.

GINGERINO seems to be at least as sensitive as currently utilised seismometers to tele-seismic events and local vibrations.

2. Raw data: the beat note frequency

The data analysis procedure is under development and tested using the GINGERINO data. Raw data consist in the laser mono-beam signals (PH1, PH2) and two beat note signals (S1, S2), from which the frequency is reconstructed and purified of the laser dynamics disturbances and systematics. In Figure 5 the beat note signal is shown.

The beat note signal S has the form $S = A + B \cdot \cos(\omega_m t + \phi_n)$, where A is an offset, B is a proportionality constant, ω_m is connected to ω_s, t is time and ϕ_n is a small noise term, such quantities are determined by the physics of light interference, and generally change with time. The reconstruction is based on the Hilbert Transform (HT), allowing the evaluation of B and ω_m as functions of time. The Matlab HILBERT function is utilized to retrieve ω_m from the raw signal. The signal (minus its offset) is first processed by a band pass filter (280 ± 50 Hz), then the HILBERT function identifies the signal amplitude (B) and phase ($\omega_m t + \phi_n$) terms. The phase term is time derived, and multiplied by the acquisition rate, in order to obtain ω_m. A full description of GINGER data analysis can be found in references [Di Virgilio et al., 2019] and [Di Virgilio et al., 2020].

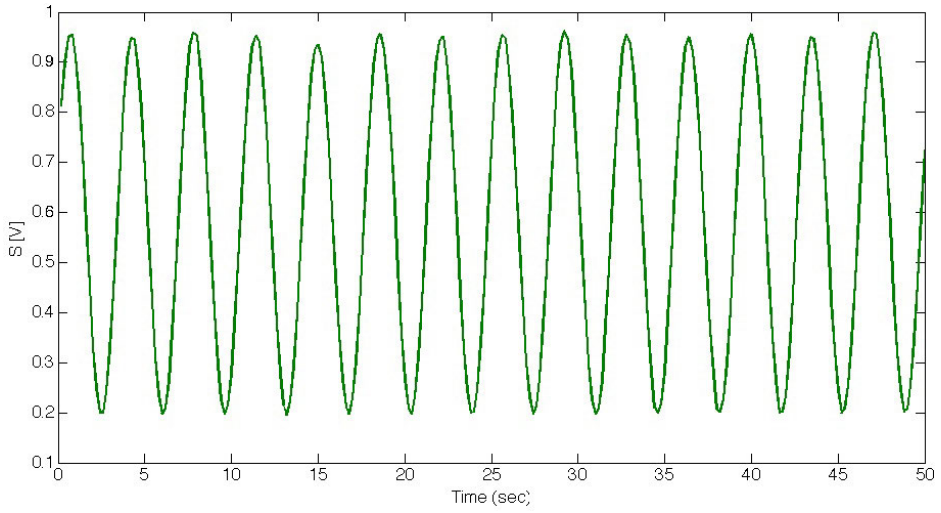

Figure 5. The beat note signal "S" detected by GINGERINO; its form "$S = A + B \cdot \cos(\omega_m t + \phi_n)$" is determined by the physics of light interference.

2.1 Typical disturbances, and data quality

Purpose of the analysis is to eliminate the systematics induced by backscattered light and laser dynamics, and identify the portion of data not suitable for the analysis, usually referred to as 'mode jumps' (very fast spikes, affecting data for a few seconds) and 'split modes' (these disturbances last for hours, but can be eliminated by geometry control); typically, about 10% of the data are removed in a free running device, when the geometry is controlled the duty cycle is 100% [Maccioni et al., 2022]. The rotational velocity obtained from the beat note pulsation, $\Omega_z = \frac{\omega_m}{2\pi S}$ (Eq. 1), is shown in Fig. 6 in presence of a mode jump. Such disturbance affects the measurement of Ω_z at the level of a few nrad/s; the mean value is subtracted.

Contrast is taken into account for determining the goodness of data, it has been defined as:

$$C = \frac{max - min}{max}, \tag{2}$$

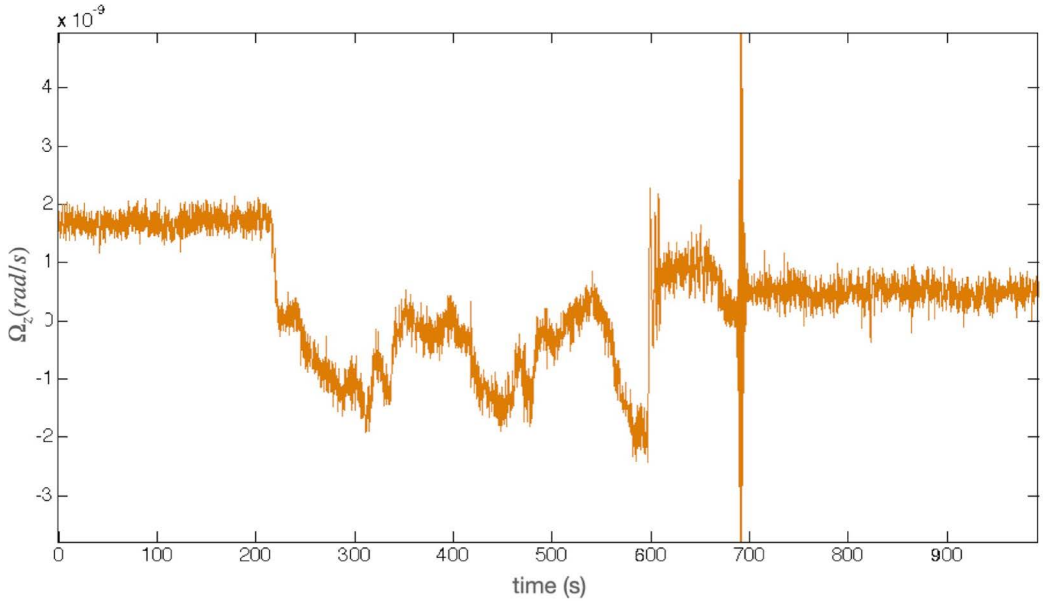

Figure 6. Ω_z derived from ω_m; its mean value is subtracted, disturbance effects are visible at the nano-rad/s level.

where "max" and "min" are the local maxima and minima of the beat note signal, Fig. 5. Alarms are implemented, in order to alert the software user every time $C < C_{min}$ (typically $C_{min} \sim 0.5 \div 0.6$) for a period greater than a few seconds (current choice is 3 seconds).

3. ω_{s0}, the fast approximation of ω_s

The main problem of RLG signal is the backscattering effect, due to mirror imperfections. In a first order approximation [Di Virgilio et al., 2019], the Sagnac pulsation can be written as:

$$\omega_s \simeq \omega_{s0} + \omega_{ns} \tag{3}$$

where ω_{s0} is constructed from the available raw signals and accounts for the backscattering, while ω_{ns} is the "null shift" term, including non linear laser dynamics. More details, for what concerns the derivation of ω_{s0} can be found in [Di Virgilio et al., 2019] and [Di Virgilio et al., 2020]; here we recall that ω_{s0} can be directly calculated from measured quantities as:

$$\omega_{s0} = \frac{1}{2}\sqrt{\frac{2I_{S1}I_{S2}\omega_m^2\cos(2\epsilon)}{I_1 I_2} + \omega_m^2} + \frac{\omega_m}{2}, \tag{4}$$

where $I_{1,2}$ are the mono-beam amplitudes filtered at low frequency, $I_{S1,S2}$ their amplitudes demodulated at the Sagnac frequency, and ϵ is the dephasing between the two mono-beams. In particular, in order to obtain $I_{1,2}$, the low pass filter was set to 50 Hz, and to demodulate at the typical Sagnac frequency the band pass filter was set to (280 ± 50) Hz. The HILBERT transform is utilized to identify amplitude and phase from raw data, as described in [Di Virgilio et al.,2019]. A schematic overview of the ω_{s0} term production is shown in Figure 7.

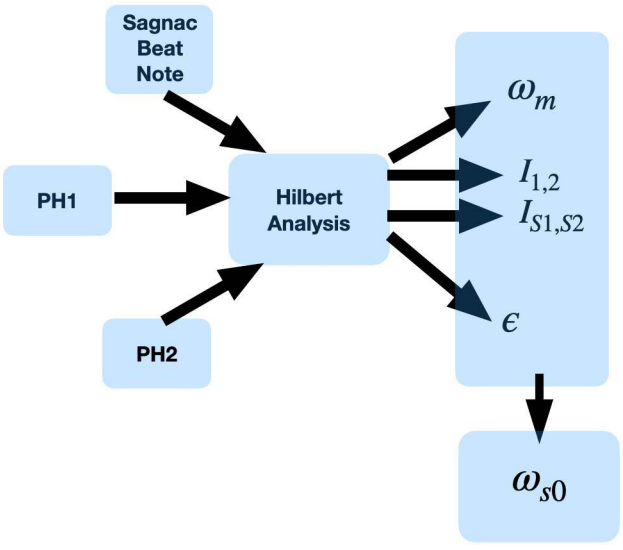

Figure 7. Schematic view of ω_{s0} production. PH1 and PH2 are the laser mono-beams raw data.

At the present moment, the delay in real time production of ω_{s0} is ~10 s, and it can be made as small as 1 s. To derive Ω_z, (Eq. 1) if ω_* is a product of the analysis (i.e. $\omega_m, \omega_{s0}, \omega_s$), Ω_z can be derived as $\Omega_z\left(\frac{rad}{s}\right) = \frac{\omega_*(Hz)}{2\pi S} \simeq \frac{\omega_*(Hz)}{2\pi \cdot 5.687 \cdot 10^6}$.

4. Ginger analysis procedures

The GINGERINO data analysis procedures consist in:

- a "light" procedure, frequency window from 10 mHz up to 100 Hz, produces ω_{s0}, which approximates ω_s in this frequency band.
- a "full" procedure: ω_s is recovered, see Eq. 3, subtracting offline ω_{ns}, for this purpose it is required to use statistical means to evaluate the optical cavity losses. This procedure is still under development.

Using the available data, it has been checked that the error in using ω_{s0} in place of ω_s is of the order of nrad/s.

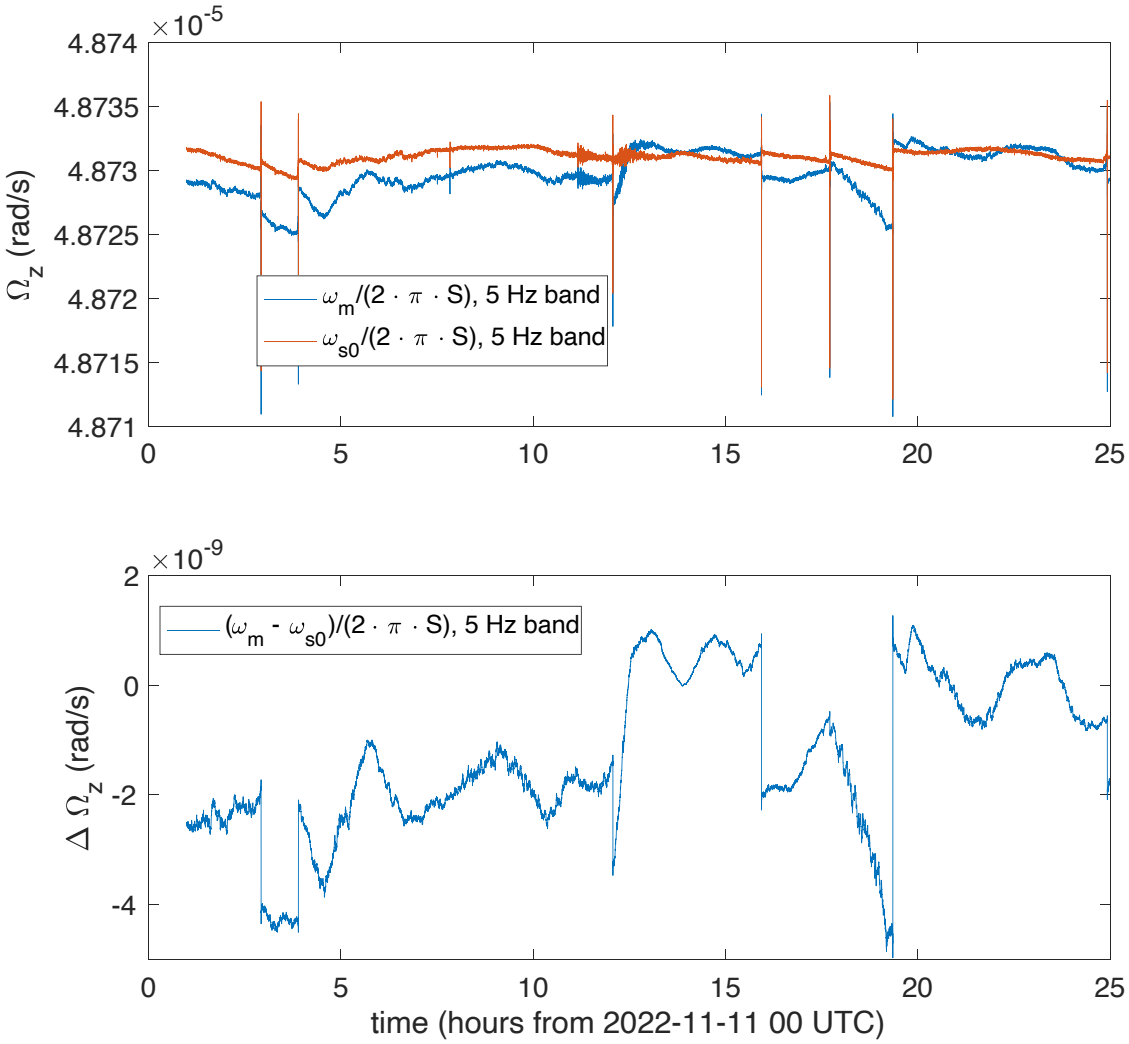

Figure 8. Comparison of Ω_z derived from ω_m and ω_{s0} (above), and their difference (below), on one day of data; time is in hours, counting from the beginning of the day. Mean values are not subtracted, in order to show the dominant Earth angular velocity.

Taking into account that typically teleseismic events are of the order of 100 nrad/s, utilizing ω_{s0} means an error of a few percent. In Figure 8 one day of data affected by a few disturbances is evaluated by means of ω_{s0} and ω_m; by solving for the backscattering, laser instabilities are mitigated. The dominant term is the Earth angular velocity as seen by Gingerino, and its mean value is compatible with a RLG horizontal within a few mrad [Di Virgilio et al., 2020]. Their difference is also shown, it can generally rise up to ~10 nrad/s.

In Figure 9, Ω_z obtained from ω_m, ω_{s0}, and ω_s is shown for a particular data set. A complete evaluation of the ω_{s0} sensitivity, and improvement with respect to ω_m, is reported in [Di Virgilio et al., 2019].

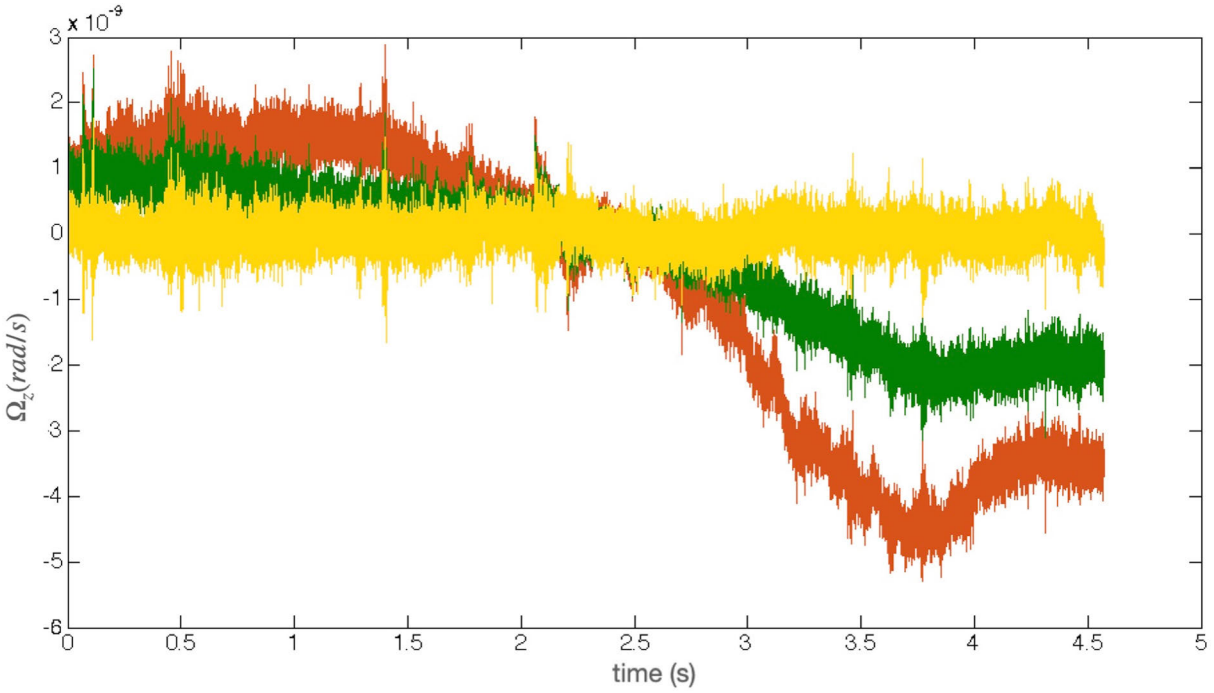

Figure 9. Plot of Ω_z derived from ω_m (orange), ω_{s0} (green), and ω_s (yellow). Since ω_s is the closest evaluation of the Sagnac frequency among the three, the improvement in using ω_{s0} in place of ω_m in the "light" procedure is shown.

5. Timing precision

For geophysics data analysis, GINGERINO is connected to a Nanometrics Centaur data logger, sampling rate 2 kHz, timing accuracy $< 100\ \mu s$ if connected to a local NTP server [Centaur Data Sheet]. As for precision in timing, crucial for frequency measurements, an upper bound was set. Timing precision was evaluated by comparing signals from two different DAQ systems, which acquire data from GINGERINO: the Centaur and the PXI. The measured beat note frequencies, $f_m = \frac{\omega_m}{2\pi}$, from the two DAQ systems, were synchronized utilizing the cross-correlation, and then subtracted. The remaining part, δf_m, could be then considered as noise; by ascribing it completely to time precision issues in the Centaur DAQ system, it was possible to set an upper bound to time precision issues. On one hand, simulations of time jitter noise were produced; a sampling rate of 2 kHz means time steps $t_{st} = 500\ \mu s$. Steps of length $t_{st} + \delta t$ have been produced, where δt is a random noise of the order of fractions of μs. By injecting such noise in an ideal beat note signal, it was possible to obtain a linear relationship between the standard deviation of the ideal f_m disturbed by the time jitter and the standard deviation of the time jitter:

$$std(f_m) = k_{jit} \cdot std(\delta t), \tag{5}$$

with $k_{jit} \sim 0.38 \frac{mHz}{\mu s}$. On the other hand, after subtracting the signal between the two DAQs, we obtained $std(\delta f_m) \sim 0.044$ mHz. An upper limit to time jitter noise of ~0.12 μs every sampling step of 500 μs was evaluated, and confirmed by a dedicated simulation.

6. Conclusions and perspectives

A dedicated data analysis procedure has been implemented to produce quasi real time GINGERINO data useful for seismology studies, providing the measurement of the rotational component of earthquakes, around the vertical

axis. The first order term, ω_{s0}, of the Sagnac pulsation ω_s is perfectly suitable for seismological investigation with an error of few nrad/s; at the present moment, the delay in real time production of ω_{s0} is ~10 s, and it can be made as small as 1 s. ω_{s0} will soon be uploaded on EIDA in place of the previously provided ω_m. Automatization of the whole process is in progress, in order to upload analyzed data on EIDA platform by means of a dedicated plugin, in real time. Moreover, training and utilization of Neural Networks (NNs) is scheduled for the next future; NNs will be trained to produce ω_{s0} from raw.

Acknowledgements. We acknowledge INFN, "Istituto Nazionale di Fisica Nucleare" for funding the GINGER experiment; raw data from the laser signals are not public, pre-analyzed data (namely, the ω_{s0}) will be available on EIDA platform, as rotational component of the IV.GIGS seismic station.

References

Belfi, J. et al. (2017). Deep underground rotation measurements: GINGERino ring laser gyroscope in Gran Sasso, Rev. Sci. Instrum. 88, 034502, https://doi.org/10.1063/1.4977051

Bernauer, F. et al. (2021). Rotation, Strain and Translation Sensors Performance Tests with Active Seismic Sources, 21,264, https://doi.org/10.3390/s21010264

Centaur Data Sheet, URL: https://nanometrics.ca/hubfs/Downloads/Data%20Sheets/Centaur_Data_Sheet.pdf?hsLang=en-ca

Di Virgilio, A., N. Beverini, G. Carelli, D. Ciampini, F. Fuso and E. Maccioni (2019). Analysis of ring laser gyroscopes including laser dynamics, Eur. Phys. J. C. 79, 573, https://doi.org/10.1140/epjc/s10052-019-7089-5

Di Virgilio, A., N. Beverini, G. Carelli, D. Ciampini, F. Fuso, U. Giacomelli, E. Maccioni and A. Ortolan (2020). Identification and correction of Sagnac frequency variations: an implementation for the GINGERINO data analysis, Eur. Phys. J. C., 80, 163, https://doi.org/10.1140/epjc/s10052-020-7659-6

https://www.rotational-seismology.org/

Igel, H. et al. (2021). ROMY: a multicomponent ring laser for geodesy and geophysics, Geophys. J. Int., 225, 684-698, doi:10.1093/gji/ggaa614

Maccioni, E. et al. (2022). High sensitivity tool for geophysical applications: a geometrically locked ring laser gyroscope, Applied Optics, 61, 31, 9256-9261, https://doi.org/10.1364/AO.469834

Simonelli, A. et al. (2016). First deep underground observation of rotational signals from an earthquake at teleseismic distance using a Large Area Ring Laser Gyroscope, Ann. Geophys., https://doi.org/10.4401/ag-6970

Simonelli, A., H. Igel, J. Wassermann, J. Belfi, A. Di Virgilio, N. Beverini, G. De Luca and G. Saccorotti (2018). Rotational motions from the 2016, Central Italy seismic sequence, as observed by an underground ring laser gyroscope, Geophys. J. Int., 214, 1, 705-715, https://doi.org/10.1093/gji/ggy186

Simonelli, A., G. De Luca, U. Giacomelli, G. Terreni and A. Di Virgilio (2020). Observation by Means of An Underground Ring Laser Gyroscope of Love Waves Generated in the Mediterranean Sea: Source Direction and Comparison with Models, Seismol. Res. Lett. 91, 1730-1737, doi: 10.1785/0220190362

Simonelli, A. et al. (2021). Monitoring Local Earthquakes in Central Italy Using 4C Single Station Data. Sensors, 21, 4297, https://doi.org/10.3390/s21134297

Yuan, S. et al. (2020). Six Degree-of-Freedom Broadband Ground-Motion Observations with Portable Sensors: Validation, Local Earthquakes, and Signal Processing, Bull. Seismol. Soc. Am., 110, 3, 953-969, https://doi.org/10.1785/0120190277

Zembaty, Z., F. Bernauer, H. Igel, K. U. Schreiber Rotation Rate Sensors and Their Applications (2021). Sensors, 21, 5344, https://doi.org/10.3390/s211653442021

***CORRESPONDING AUTHOR: Simone CASTELLANO**,
Gran Sasso Science Institute, L'Aquila, Italy
e-mail: simone.castellano@gssi.it